Ocean Deployment and Testing of a Semi-Autonomous Underwater Vehicle

Nicholas R.J. Lawrance, Thane Somers, Dylan Jones, Seth McCammon and Geoffrey A. Hollinger

Robotics Program, School of Mechanical, Industrial, and Manufacturing Engineering,

Oregon State University, Corvallis, OR 97331

Email: {nicholas.lawrance, somersth, jonesdy, mccammos, geoff.hollinger}@oregonstate.edu

Abstract—We present the design overview and navigation performance for an offshore deployment of a semi-autonomous underwater vehicle (sAUV). The system is based on a commercially-available observation class remotely operated vehicle (ROV), combined with a commercial AUV navigation system. The vehicle also has onboard visual cameras, a Doppler velocity log, and a multibeam imaging sonar. We present the integration of the various subsystems as well as a Robot Operating System (ROS)-based interface that allows researchers to visualize sensor and navigation data and send commands to the vehicle in real time. Results from an April 2016 offshore trial are presented, demonstrating the station keeping and waypoint following capabilities of the vehicle in open water.

I. Introduction

Underwater robotic vehicles provide inspection and data collection capabilities without the need for humans to operate underwater. They can be classified into two categories based on autonomy level, remotely-operated vehicles (ROVs) require constant human control whereas autonomous underwater vehicles (AUVs) provide a degree of automatic control without the need for a human operator. The application domains tend to overlap, although very long-duration vehicles such as ocean gliders tend to be autonomous [1] and many inspection vehicles are remotely-operated because an operator is required to understand the inspection task.

Until recently, the high cost of underwater platforms has limited their use to large research institutes and corporations. This has meant that vehicles were generally custom-built. Recent developments have introduced lower-cost, more accessible vehicles. This has reduced the barriers to deploying underwater robots for routine inspection and data collection tasks usually performed by human divers. These tend to be shallow-water (<100 m) operations performed in off-shore marine or freshwater environments. However, operating in shallow marine environments requires contending with disturbances from ocean waves and currents. This paper presents work towards the development of a low-cost semi-autonomous underwater vehicle (sAUV) that provides limited autonomy but is based on a commercial ROV platform.

While ROVs are a relatively mature technology, they are still costly to operate due to the requirement for constant human control. Human operation of ROVs is particularly challenging because it requires a high degree of operator training and skill, and the constant attention can be draining to a human operator. In order to reduce operator load, ROVs are a strong candidate
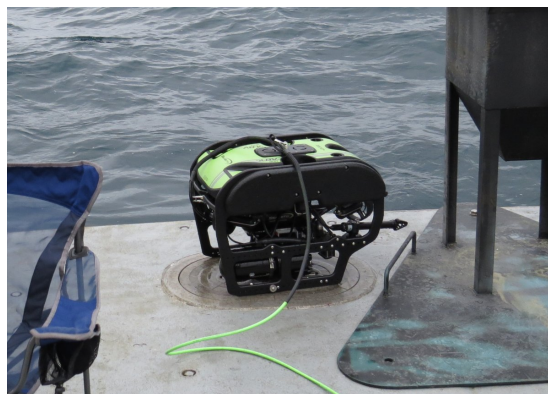

Fig. 1. Semi-autonomous underwater vehicle (sAUV) in preparation for deployment near Newport, OR.

for introducing autonomy to reduce operator load in simpler tasks, such as station keeping and traveling between known positions. While these tasks are routine for autonomous surface and aerial vehicles, the challenges of underwater navigation and communication have reduced the number of deployed autonomous underwater vehicles [2], [3].

We demonstrate the operation of a low-cost platform developed primarily from commercially-available components with a total value of approximately $150k. This is significantly less than existing solutions that cost over $500k [4]. We also present a software interface based on the popular open-source Robot Operating System (ROS) that allows a user to visualize the robot in real-time, access data streams, and send basic commands to the robot. We also provide the results of basic navigation and control, including station keeping and waypoint following. We found that the vehicle was affected by wave forces at 10 m depth, and strong currents persisted down to 40 m depth, affecting the control capabilities of the vehicle.

II. System overview

The system is based on the Seabotix vLBV300 observation-class [5] ROV platform. The vLBV300 is a small tethered vehicle with a dry mass of approximately 19.0 kg given minimal sensor load. In the current configuration with a full sensor load, the vehicle has a dry mass of 36.2 kg, including 2.0 kg of ballast for operation in seawater. The vehicle is rated to a depth of 250 m and has a 350 m tether. This tether provides both power and communications with the vehicle through an Ethernet and serial interface. The vLBV300 platform is

Fig. 2. sAUV control station, including sonar visualizer (far left, 1), Greensea navigation console (2), manual control console (3), ROS data interface (4) and ROS rviz visualization (5).

(a) Navigation visualization.   (b) Depth GP model.

Fig. 3. ROS visualization using the rviz package. The ROS based interface displays live navigation data to visualize the robot pose (3a) and process sensor data. A simple bathymetry estimator is shown in 3b that uses GP regression from DVL depth estimates (grey cones), where the colors of the base map indicate uncertainty.

a vectored thrust vehicle with six thrusters. Two vertically-aligned thrusters provide vertical lift, and four angled lateral thrusters provide horizontal in-plane motion and rotation. The vehicle is passively stable in roll and pitch, and thus in normal use has four controllable degrees of freedom (roll is possible by providing differential thrust to the vertical thrusters but is not commonly used).
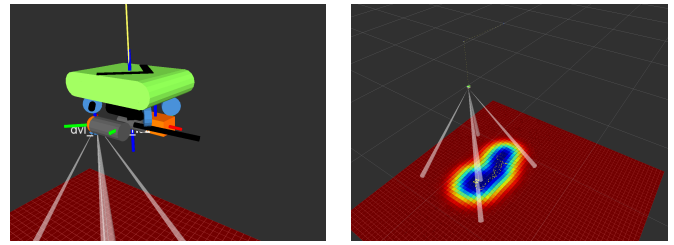
Navigation is provided by a Greensea INSpect GS3 navigation system[1]. The navigation system is primarily based on a microelectromechanical system accelerometer and gyroscope, providing three-axis acceleration and rotation rate data, and a three-axis magnetometer. The navigation system also fuses data from the onboard Teledyne Explorer Doppler velocity log (DVL) that provides lateral velocity estimates and range information. The DVL uses a four-beam phased array antenna with frequency 614.4 kHz. Finally, the vehicle has a Tritech Gemini multibeam imaging sonar that provides sonar data for underwater navigation.

III. ROS INTERFACE

We developed a ROS interface for the sAUV system to access sensor data and vehicle controls. ROS is an open-source middleware platform for controlling and developing applications for robotic systems [6]. ROS is popular in the robotics research community due to the high number of freely-available applications [7]. Currently, communications onboard our vehicle are built around the UDP network messaging protocol LCM [8]. To form a communication bridge between LCM messages and ROS, we developed the ROS software package lcm_to_ros[2]. The package takes as input LCM message definitions and generates corresponding ROS message definitions as well as autogenerated C++ code for ROS nodes that receive LCM messages from the network, convert them to ROS equivalent message types and republish them onto the ROS network. The reverse direction (ROS messages to LCM messages) is also available, allowing ROS nodes to send commands to the robot. Figure 2 shows the command interface

which using both the manufacturer-supplied controller and camera as well as the ROS interface.

By bringing data from the navigation system, sensors and manual commands into the ROS system, it becomes straightforward to generate visualizations and process sensor data. Figure 3 shows some sample images from the ocean deployment described below using the ROS rviz package [6]. A simple 3D model can be used to show the estimated vehicle position and orientation in real time. Subfigure 3b illustrates a simple application, using a Gaussian Process regression model [9] to construct an estimated bathymetry map from DVL range data. These data streams are useful for planning missions, either fully autonomously or human-aided.

IV. OCEAN DEPLOYMENT

The system was deployed for a test mission near $44.678°$ N $124.109°$ W, approximately 2 km offshore of Yaquina Head near Newport, Oregon on 20 April 2016 (see Fig. 4). The average ocean depth in this area is about 50 m. The primary goals of the deployment were to demonstrate station keeping and waypoint following capabilities in ocean conditions and to demonstrate the ROS-based interface.

The deployment was conducted from the R/V Elakha, a 54 ft Class III research vessel owned and operated by Oregon State University. The deployment consisted of two dives to conduct tests at depths ranging from the surface to approximately 45 m. Total dive time was approximately 80 minutes. During the deployment the average significant wave height was 0.7 m, corresponding to sea state 3 [10].

To illustrate wave conditions on the vehicle we collected data for approximately 5 minutes while the vehicle was left uncontrolled at the surface and at 10 m depth. We generated the nondirectional wave power spectra illustrated in Fig. 5 by analyzing the vertical displacement estimates from the navigation system, which generates position estimates at approximately 50 Hz. The power spectra were calculated using the National Buoy Data Center (NBDC) specifications [11]. This is essentially a discrete Fourier transform over the displacement data to generate estimates of the wave power as a function of frequency. The significant wave heights H_{mo} were 0.540 m and 0.394 m for the surface and 10 m depth
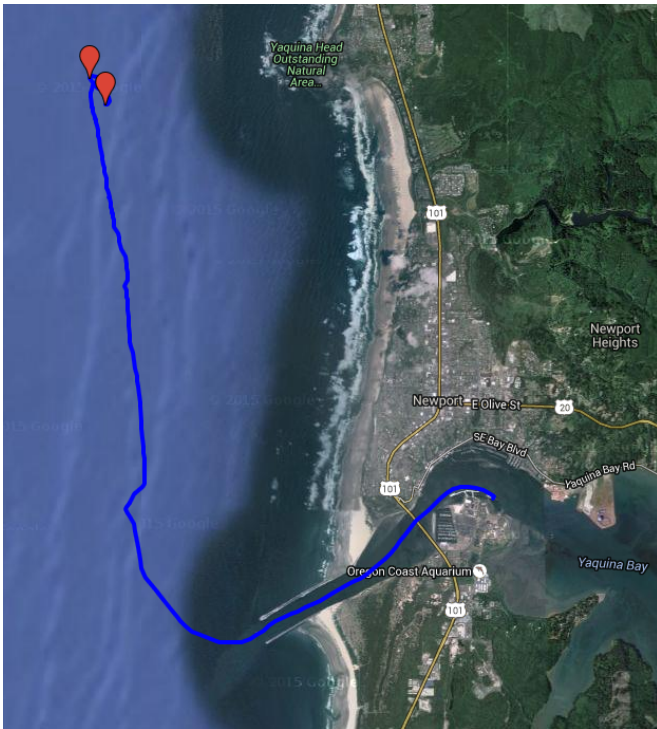
Fig. 4. Boat track showing the two dive site locations off the coast of Newport, Oregon.
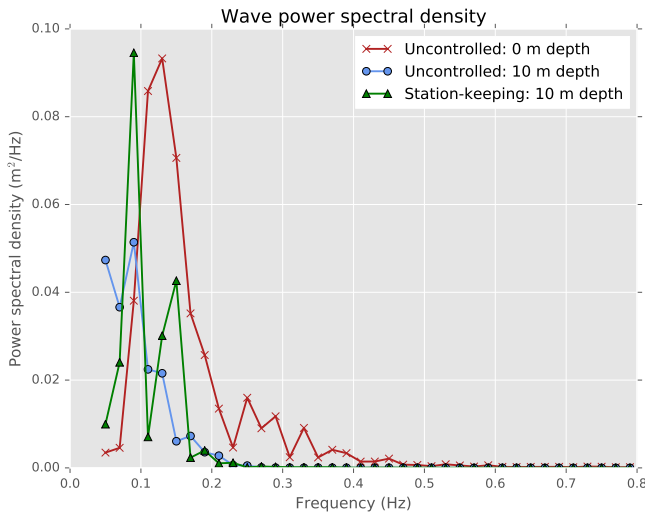

Fig. 5. Wave power spectra generated by recording vehicle vertical displacement when uncontrolled at the surface and 10m depths.

records respectively, where H_{mo} was calculated using the NDBC criterion ($H_{mo} = 4\sqrt{m_0}$), with m_0 being the first moment of the power spectrum.

Figure 5 shows that the wave perturbations reduce with depth. In particular the higher-frequency components are almost completely damped out. This can be explained partly by the effect of the decrease in wave power with depth, and partly because when the vehicle is at the surface it is only partially submerged, so the drag profile is different from when it is fully
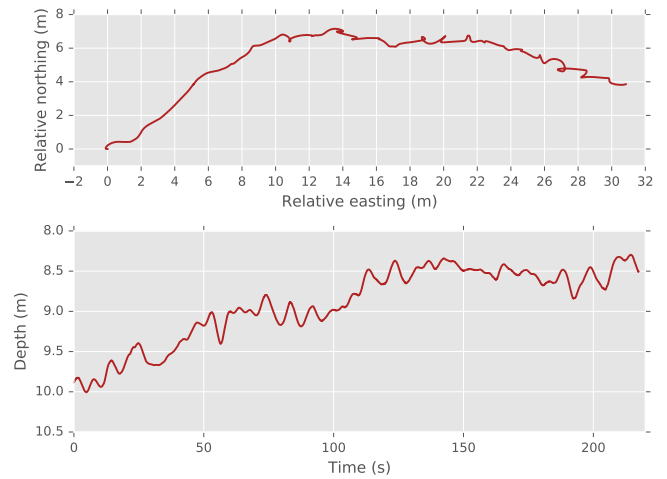

Fig. 6. Uncontrolled vehicle displacement at 10m depth.

immersed. In general though, there are still significant wave effects from lower frequency waves, especially around the 0.1 Hz frequency range. There was also a noticeable current during the record at 10 m depth. Figure 6 shows the drift of the vehicle in lateral coordinates (equating to an easterly drift of approximately 0.14 m/s) as well as the vertical displacement. Note that to aid in the recovery of the vehicle, it was ballasted for slight positive buoyancy. When left uncontrolled it floated towards the surface at approximately 7 mm/s. These results allow us to characterize the station keeping performance of the vehicle.

V. NAVIGATION PERFORMANCE

One of the primary goals of the offshore deployment was to analyze the navigation performance of the vehicle. In particular, we were interested in how well the vehicle would perform at different depths, under the varying effect of wave forces (which tend to decrease with depth) and ocean current forces. During the offshore trial we collected data while the sAUV was uncontrolled, attempted to station keep at a single position, and performed lateral square patterns to characterize the uncontrolled and controlled performance of the vehicle. We used the standard (closed-loop linear PID) controllers supplied with the navigation system with no custom gain tuning.

A. Station keeping

Station keeping is a useful autonomous operation for an sAUV because it provides a non-expert user the ability to keep the vehicle stationary, providing easier visual inspection and manipulation capabilities. Our future work is aimed at generating relative-control shared autonomy, where the vehicle can automatically maintain a fixed (earth-frame) position in the presence of disturbances and currents, and the user can input relative position commands. To characterize the position-hold performance, we performed station keeping at depths of 10 m and 40 m. In each station keeping data set shown, the vehicle was commanded to remain at a fixed position and
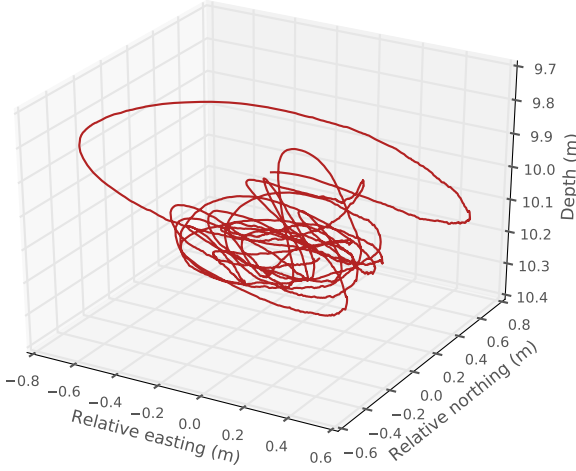
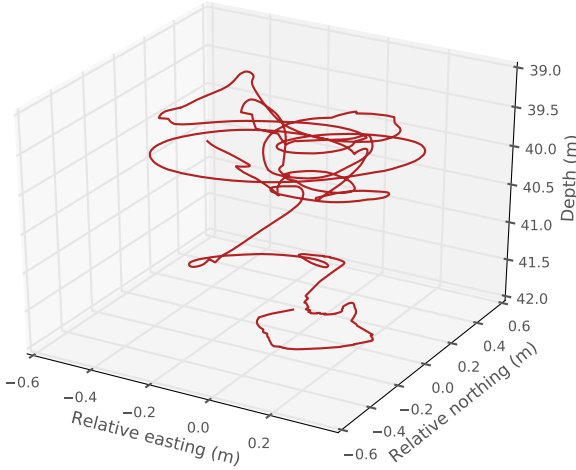Fig. 7. Station keeping vehicle displacement at 10m depth.

Fig. 8. Station keeping vehicle displacement at 40m depth.

	RMSE		Mean error	
	10 m	40 m	10 m	40m
Northing (m)	0.276	0.206	0.223	0.177
Easting (m)	0.191	0.185	0.146	0.145
Depth (m)	0.105	0.729	0.083	0.636
Heading (°)	1.181	1.101	0.888	0.873

response with station keeping turned on in Fig. 5 using the z-axis motions during station keeping. Note that there was still a large response at low frequencies, though the overall equivalent 'significant wave height' (a measure relating to the total energy from the wave perturbations) is reduced to 0.323 m when station keeping compared to 0.394 m when uncontrolled. These results suggest that the controller could be tuned to have the required frequency response, or a predictive controller could be used to reduce wave disturbances [12].

Figure 8 and Table I show the position traces and errors for station keeping performed at 40 m depth for approximately 165 s. The results were similar to the 10 m depth results, but showed a larger tracking error in the vertical displacement. We suspect this was caused by turbulence from the thrusters because the vehicle was close to the seabed (altitude < 3 m). We also noticed that at low altitudes sediment disruption was visible in the cameras when the vertical thrusters were active.

B. Waypoint following

We were also interested in characterizing the sAUV's capability for navigating between earth-frame fixed waypoints. We performed commanded box patterns of 3 and 10 m sidelengths at 10 and 40 m depths. Figure 9 illustrates the internal position estimate of the vehicle during execution of a 3 m square pattern at 10 m depth over approximately 120 s. The heading is indicated by the orange arrow symbols which are shown every 5 seconds of the trajectory. The commanded heading was bearing 0 (North). The results show that the controller could reach and traverse between waypoints to within approximately 1 m with respect to the internal navigation solution. The 10 m box pattern at 10 m depth is shown in Fig. 10, where the total time of the pattern was approximately 310 s. The position error increased with the larger box because the vehicle reached higher speeds during the edge transitions resulting in larger overshoot at the corners. There was also a period where the navigation system filters diverged and the controller was deactivated (shown as blue dots). During this time the vehicle drifted for around 10 s before the controller was reactivated.

Figures 11 and 12 show the same 3 and 10 m box patterns respectively at 40 m depth. The mission lengths were 220 and 400 s respectively. The performance is roughly similar to the 10 m depth results. However, note that in the 10 m box results (Fig. 12) there was a relatively strong east-moving current. This can be seen in the speeds of the east-west versus west-east transitions (note the spacing of the five-second interval
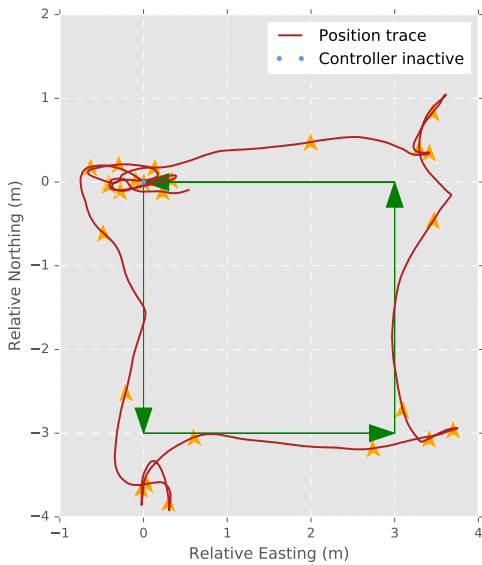
heading and allowed to reach a relatively stable state before data collection. Note that the position and orientation data is from the navigation system, which is generated by fusing the DVL and INS sensor measurements.

The displacement of the vehicle during a 150 s period of station keeping at 10 m depth is shown in Fig. 7, recorded shortly after the 10 m uncontrolled data seen in the previous section. Table I shows the position errors during station keeping, using the standard definitions of root mean square (RMS) and mean errors. It is interesting to note that although the position hold worked relatively well (resulting in a maximum distance from the target position of 0.88 m) compared to the drifting seen in Fig. 6, there were still significant perturbations caused by the wave motion. The controller was not particularly well-tuned to rejecting wave disturbances, resulting in some of the low frequency wave perturbations still being present. To highlight this, we have shown the equivalent frequency

Fig. 9. Vehicle moving around a commanded 3 m square pattern at 10 m depth. The vehicle started at $(0, 0)$ and followed the waypoint order indicated by the green arrows with a constant North heading command.
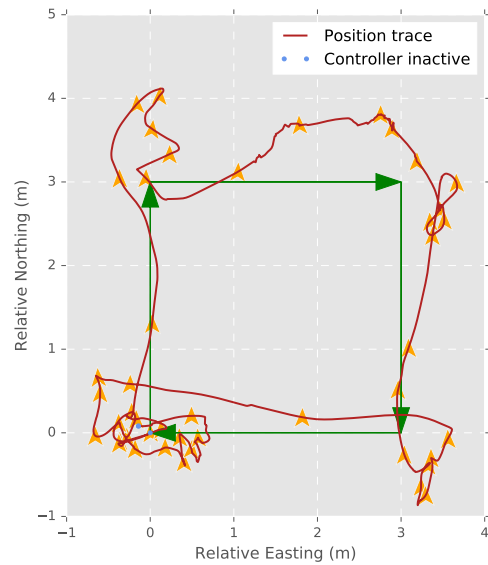

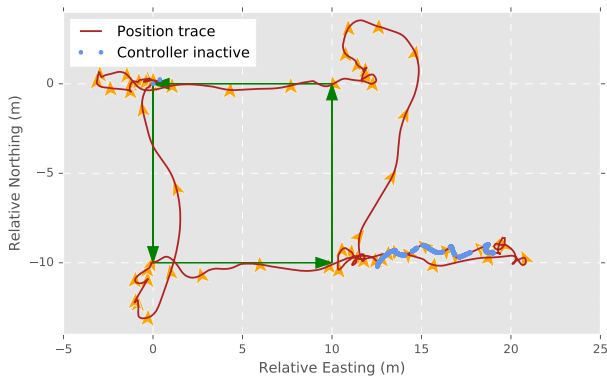Fig. 11. Vehicle moving around a commanded 3 m square pattern at 40 m depth.

Fig. 10. Vehicle moving around a commanded 10 m square pattern at 10 m depth.

Fig. 12. Vehicle moving around a commanded 10 m square pattern at 40 m depth.

arrows). The current also caused a sustained bearing tracking error during the east-west transition. In the 10 m box case there was a short (5 s) navigation failure near the north-west corner of the box because the DVL lost bottom lock when vehicle was very close to the sea floor. Note that we were commanding a constant (pressure) depth, rather than a constant altitude, so the altitude varied between around 1 and 5 m during the mission.

VI. CONCLUSION

We presented the design and testing of a small, cost-effective, semi-autonomous underwater vehicle. Assembled from off-the-shelf hardware and a mix of OEM and custom software, the sAUV records data from sonar and visual cameras and is capable of basic navigation using an INS, magnetometer and DVL. We developed the ROS package lcm_to_ros, an interface that parses LCM messages to and from the navigation system and converts them to native ROS
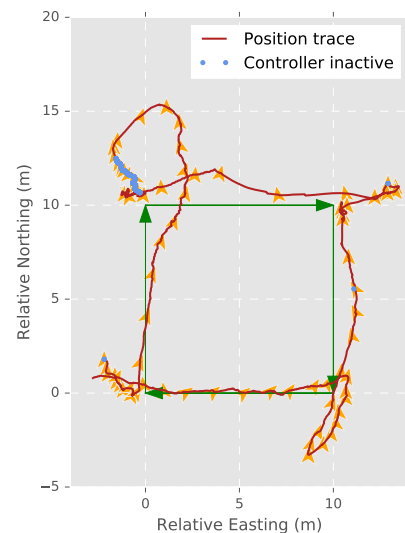
messages for use with ROS packages. We tested the system on an ocean deployment and demonstrated station keeping and waypoint following. We found that the station keeping was capable of maintaining a position to within approximately 1 m but was still affected by low-frequency perturbations from wave forces down to at least 10 m depth. We also demonstrated waypoint following at 10 m and 40 m depths and found that the vehicle could reach target waypoints but suffered from overshoot and occasional navigation failure, from which the vehicle recovered well.

VII. FUTURE WORK

Obtaining an external 'ground truth' navigation estimate is especially challenging for underwater vehicles [2]. To attempt to characterize the navigation performance, during the deployment we performed a set of maneuvers near the sea floor (altitude < 5 m) with visible sonar features. Future work will attempt to use this information to generate independent navigation estimates to validate the navigation performance. We are also considering online mapping during flight using features from the sonar to improve navigation performance. Finally, in future deployments we will work on a more thorough analysis of controllers to attempt to reduce the disturbance from wave motions. Alternative control methods may also need to be considered given the low-frequency disturbances from waves at shallow depths.

ACKNOWLEDGMENT

REFERENCES

[1] J. Sherman, R. E. Davis, W. B. Owens, and J. Valdes, "The autonomous underwater glider "Spray"," *IEEE Journal of Oceanic Engineering*, vol. 26, no. 4, pp. 437–446, Oct 2001.

[2] L. Paull, S. Saeedi, M. Seto, and H. Li, "AUV navigation and localization: A review," *IEEE Journal of Oceanic Engineering*, vol. 39, no. 1, pp. 131–149, 2014.

[3] L. Freitag, M. Grund, S. Singh, J. Partan, P. Koski, and K. Ball, "The WHOI micro-modem: an acoustic communications and navigation system for multiple platforms," in *Proc. MTS/IEEE OCEANS*, 2005, pp. 1086–1092.

[4] J. Vaganay, M. Elkins, D. Esposito, W. O'Halloran, F. Hover, and M. Kokko, "Ship hull inspection with the HAUV: US navy and NATO demonstrations results," in *Proc. MTS/IEEE OCEANS*, Sept 2006, pp. 1–6.

[5] R. D. Christ and R. L. Wernli Sr., *The ROV manual: a user guide for remotely operated vehicles*, 2nd ed. Butterworth-Heinemann, 2014, pp. 5–7.

[6] M. Quigley, K. Conley, B. Gerkey, J. Faust, T. Foote, J. Leibs, R. Wheeler, and A. Y. Ng, "ROS: an open-source robot operating system," in *ICRA Workshop on Open Source Software*, 2009.

[7] S. Cousins, "Exponential growth of ROS," *IEEE Robotics & Automation Magazine*, vol. 1, no. 18, pp. 19–20, 2011.

[8] A. S. Huang, E. Olson, and D. C. Moore, "LCM: Lightweight communications and marshalling," in *Proc. IEEE/RSJ International Conference on Intelligent Robots and Systems*, 2010, pp. 4057–4062.

[9] C. E. Rasmussen and C. K. Williams, *Gaussian Processes for Machine Learning*, ser. Adaptive computation and machine learning. Cambridge, Massachusetts: The MIT Press, 2006.

[10] Secretariat of the World Meteorological Organization, "Manual on codes - international codes; part A - alphanumeric," World Meteorological Organization, Tech. Rep. WMO-No. 306, 1995.

[11] M. D. Earle, "Nondirectional and directional wave data analysis procedures," National Oceanic and Atmospheric Administration, Tech. Rep. NDBC Technical Document 96-01, 1996.

[12] D. C. Fernández and G. A. Hollinger, "Model predictive control for underwater robots in ocean waves," *IEEE Robotics and Automation Letters*, vol. 2, no. 1, pp. 88–95, Jan 2017.